

X-RAY EMISSION MECHANISMS WITHIN THE SOUTHERN HOT SPOT OF RADIO GALAXY 3C 445

EMILY M. MAY¹

Department of Physics and Astronomy, University of Wyoming, WY 82071

ERIC S. PERLMAN

Department of Physics and Space Sciences, Florida Institute of Technology, FL 32901

DEMOSTHENES KAZANAS

Laboratory for High Energy Astrophysics, NASA Goddard Space Flight Center, Code 661, Greenbelt, MD 20771

AND

MARKOS GEORGANOPOULOS

Joint Center for Astrophysics, Department of Physics, University of Maryland, Baltimore County,
1000 Hilltop Circle, Baltimore, MD 21250

ABSTRACT

The defining feature of radio-loud active galaxies are the pairs of radio-emitting jets that flow for distances of many kiloparsecs from the center out into the intergalactic medium. These jets often terminate in regions of intensified brightness, or hot spots, that occur when the flow of the jet collides with the intergalactic medium. There is an ongoing debate in extragalactic astronomy as to the emission mechanisms in these hot spots. Here we discuss observations at X-ray and infrared wavelengths of radio galaxy 3C 445 which were centered on the approaching southern hotspot. We propose that the emission from the southern hotspot contains emission both from the synchrotron and inverse-Compton (IC) processes. Fits to the spectra of the hot spot and AGN, a contour plot in the X-ray and overlaid in the infrared, and two models for the synchrotron and IC emission within the hot spot are presented.

Subject headings: active galaxies, radiation mechanisms, X-ray, infrared, 3C 445, inverse compton, synchrotron, hot spots

1. INTRODUCTION

3C 445 is a powerful radio galaxy at a redshift $z = 0.0562$ with jets that extend for many kiloparsecs, ending at hotspots $\approx 5'$ north and south of the active nucleus. These hot spots are areas of increased brightness caused by the collision between the jet and the intergalactic medium (Harris & Krawczynski 2006). At these locations, the jet slows from relativistic speeds (bulk Lorentz factors $\Gamma \approx 2-5$) to much slower, sub-relativistic speeds (Georganopoulos 2003). Because of the shock formed by the interaction of the jet with the intergalactic medium, the hotspots are often the site of energetic phenomena, including enhanced particle acceleration. However, the overall balance of emission processes in these regions is not well known, particularly with regard to X-rays. There are two possible models we explore: the synchrotron model and the inverse-Compton (IC) model. In the synchrotron model, radiation from the hot spot is emitted by very high energy electrons gyrating in a magnetic field. The relativistic electrons interact with the magnetic field, and as they lose energy they produce synchrotron radiation in all wavebands. (Longair 1994). In the IC model, low energy photons collide with relativistic electrons, either from within the jet or external sources, including the cosmic microwave background

(CMB), exciting the photons to higher energies (Longair 1992). This also results in X-ray emissions.

In this paper, our focus will be on the southern hotspot of 3C 445, which is the brighter region, believed to be approaching us and therefore amplified by relativistic effects. This represents the first study of extended X-ray emission from this object, and we report the discovery of extended X-ray emission from the southern hotspot. It is generally not possible to explain the X-ray emission from hot spots such as this with only a single model, as the shape of their broadband spectral energy distribution has a double-humped shape, with the X-ray emission above an extrapolation of the radio-optical emission. (Hardcastle et al. 2004). We propose a model that includes both synchrotron and IC emission. In §1, we propose two models for the synchrotron and IC emission. In §2, an overview of the instrumentation used for the observations and the details of our data collection are given, and §3 discusses the data reduction followed by data analysis. Next, §4 presents the results of our spectral fitting of the hot spot and AGN. §5 gives a discussion of the hot spot results and finally, our conclusions as to the X-ray emission mechanisms of the southern hot spot are presented in §6.

2. OBSERVATIONS

Observations were taken by the Chandra X-ray Observatory in the X-ray, the Very Large Telescope (VLT) in the infrared, and the Very Large Array (VLA) in the

Electronic address: eperlman@fit.edu

¹ Southeastern Association for Research in Astronomy (SARA) NSF-REU Summer Intern (2008)

radio.

3C 445 was observed with the Advanced CCD Imaging Spectrometer (ACIS) on the Chandra X-ray Observatory on 18 October 2007 for a span of about fifteen hours. The CCD chips in ACIS convert incident X-ray events into electronic signals that record the location and energy of the event. *Chandra* observes in a Lissajous pattern, with the telescope moving so that the effect of bad pixels and the effect of the pixel size on the resolution ($0.492''/\text{pix}$) can both be minimized. In the X-rays, CCDs are also moderately sensitive to the energy of the incident photon, so that some spectral information is retained. The ACIS-S configuration was used in our data set due to its linear alignment, which allows for a longer field of view. In the alternate ACIS-I configuration the chips are arranged in a square-like pattern. The northern and southern hot spots are at projected distances of ≈ 460 kpc and ≈ 450 kpc respectively from the core of the galaxy (Prieto et al. 2002). Because these distances are so great, the S configuration was chosen so that all the events could be included in the observation.

Optical and near-infrared observations of the northern and southern hot spots were obtained by Prieto (2002) with the Very Large Telescope (VLT) of the European Southern Observatory (ESO) and the Infrared Spectrometer and Array Camera (ISAAC) in the K_S ($2.2 \mu\text{m}$), H ($1.7 \mu\text{m}$), J_S ($1.2 \mu\text{m}$), and I ($0.9 \mu\text{m}$) bands. A median filter of several adjacent frames was used for sky background removal, and the integration time ranged from 35 to 60 minutes depending on the band. Those authors also discussed radio observations taken at the Very Large Array (VLA) at multiple frequencies, which were analyzed in greater detail by Brunetti (2003).

3. DATA REDUCTION AND ANALYSIS

The greatest amount of time was spent looking at the X-ray data with the Chandra Interactive Analysis of Observations (CIAO) software package. Virtually no data preparation was necessary because our data was taken so recently. We did not need to remove afterglow events because our data was processed with SDP version 7.6.11.2. The data had already gone through Reprocessing III, so we had a Level=2 event file. We were ready to begin following the Imaging threads.

By following the Imaging threads for extended sources, we ultimately extracted spectra for the hot spot and the AGN. First, we created an exposure map (a map of the total exposure as a function of position on the sky) by combining the instrument map with the aspect histogram. The exposure map is key in data reduction because it can be used to convert the counts image of a source to an image in flux units. From this image, we found an approximation for the source flux. The instrument map is a map of the effective area as a function of position on the detector at a given energy, and the aspect histogram is the map of dwell time versus pointing direction built up by the telescope's pointing motion. Once these two were completed, the CIAO command *mkexpmap* was used to combine the two, resulting in the exposure map. The X-ray image was normalized by the exposure map to obtain an image in flux units ($\text{photons} \times \text{cm}^{-2} \times \text{s}^{-1} \times \text{pixels}^{-1}$) with *dmimiscalc*.

Next, we extracted spectra of the hot spot and AGN using *specextract*, and then fit the spectrum of the regions

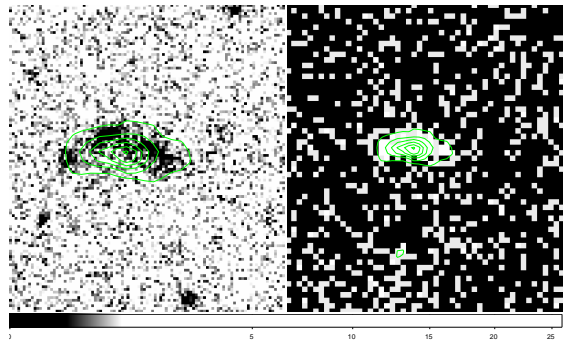


FIG. 1.— Two views of the southern hotspot of 3C 445. On the left, we show an overlay of the contours from the *Chandra* X-ray image with the VLT near-IR image shown in greyscale. On the right, we show the *Chandra* X-ray image with its flux contours overlaid. The structural differences of the hot spot at these wavelengths may reveal new information about its emission mechanisms.

in Xspec. This process is discussed in §4. Once the fitting of the spectra was complete, we moved on to the infrared data taken by the VLT. A contour plot was made of the hot spot in the X-ray and the contours were overlaid to the infrared image. This image is also presented in §4. Because there was a problem with the astrometry of the VLT image, we used an image of the same sky area from the Palomar Sky Survey to calculate the shifts in RA and dec in the VLT image and converted them to pixels. Once the astrometry was corrected, we overlaid the X-ray contours to the infrared image.

In the final stage of data analysis, two models of the emission from the hot spot were created using the Compton Sphere Suite (Georganopoulos et al. 2007). In this one-zone steady-state model, a sphere of a given radius is being permeated by a magnetic field. A power law electron distribution function is continually being injected into the sphere as it moves with a given Lorentz factor through an external photon field with an assumed black body spectrum. The electrons experience synchrotron and IC losses before leaving the source, and our model calculates both at a point where the system reaches a steady state. In the alpha version that we used, IC losses are treated as a continuous process. Initial values for the calculation of the model spectrum were taken from Prieto et al. (2002).

In Figure 1, the contours of the hot spot are shown in the X-ray and then overplotted with the VLT infrared image. Note the differences in the structure of the hot spot in the X-ray versus the infrared. In the X-ray there appears to be only one region, whereas in the infrared there are three distinct regions. The X-ray region can basically be described as a filled semicircle whose peak density does not align with any of the three bright regions in the infrared image. These three regions form an arc-like pattern which is typically the structure of a post-shock region most often seen in radio waves (Prieto et al. 2002). We discuss the difference in these morphologies further in §5.

4. SPECTRAL FITTING RESULTS

We extracted spectra for the AGN and southern hotspot of 3C 445, using *specextract* in CIAO. In order to create the spectra of the hot spot and the AGN, we defined three regions in ds9: the hot spot, the AGN, and a background region. We examined the Chandra image,

creating two separate regions that included only the hot spot and only the AGN. We chose a background region that was free from other sources in the image to get an accurate representation of the sky background. These three regions defined which area in the Chandra data file to use with *specextract*. This allowed us to create a series of files for both the hot spot and the AGN, including source and background PI spectra, weighted ARF, RMF files, FEF weight files, and a grouped spectrum for each source. The energy range was left unrestricted for both source spectra. Once the spectra were completed, so was our data analysis in CIAO. Following this step, Xspec was used to fit both the spectra of the hot spot and the AGN. The results of both spectra are presented below.

4.1. Southern Hot Spot Fit

The southern hot spot was easily modeled by a basic power law with fixed galactic absorption $N_H^{Gal} = 5.33 \times 10^{20} \text{ cm}^{-2}$, which is the same galactic absorption used for the AGN fit as presented in Table 1. Our best fit resulted in a photon index $\Gamma = 1.95^{+0.38}_{-0.34}$ and a χ^2 value of 0.85 and is shown in Figure 2. Due to the very low number of counts in the X-ray data for the hot spot, the error bars are rather large on the spectrum itself. This is to be expected because the southern hot spot is relatively dim.

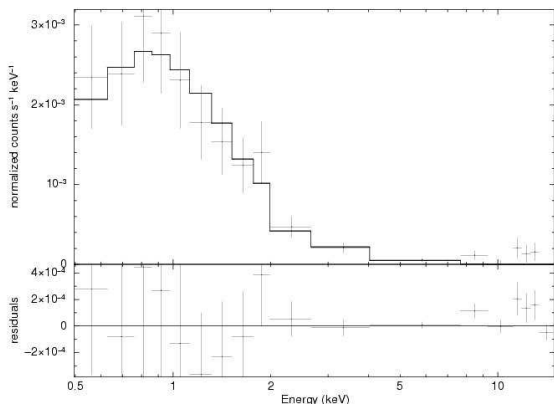


FIG. 2.— Here is the spectrum of the southern hot spot with the best fit power law overlaid. Below it are the residuals.

4.2. AGN Fit

The fit of the AGN spectrum proved to be far more complicated than that of the hot spot. Our best fit of the AGN spectrum is given in Figure 3. The final fit includes three power laws with tied photon indices absorbed by N_H^1 , N_H^2 , and N_H^3 , cold reflection modeled by *pe xrav*, and four gaussian components to represent the FeK α and O3 emission lines present in the spectrum. Although we did follow the procedure of Sambruna et al. (2007), our fit is slightly different. We did not use XSTAR, and we added four gaussian components to account for the clearly seen FeK α and O8 emission lines that were not present in the Sambruna et al. paper.

Mimicking the model presented by Sambruna (2007), our model of the AGN included three power laws with absorbers, cold reflection modeled by *pe xrav*, and four

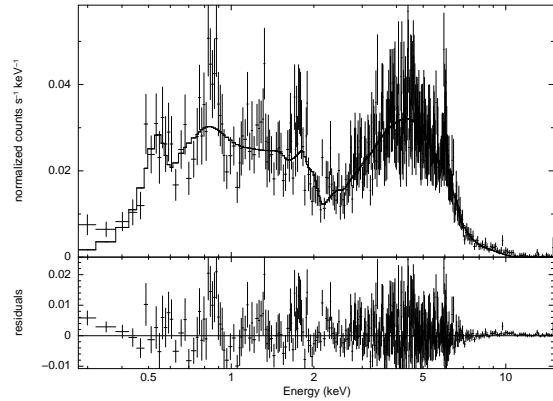


FIG. 3.— The spectrum of the AGN is shown with the best fit (a power law with three absorbers, cold reflection, gaussian components and galactic absorption) overlaid. Below it are the residuals.

TABLE 1
XSPEC AGN BEST FIT
PARAMETERS

Parameter	Value
N_H^{Gal}	$5.33 \times 10^{20} \text{ cm}^{-2}$
N_H^1	$18.8 \times 10^{22} \text{ cm}^{-2}$
Γ_1	$2.6^{+0.16}_{-0.19}$
N_H^2	$2.7 \times 10^{22} \text{ cm}^{-2}$
Γ_2	$-0.89^{+0.06}_{-0.05}$
$\Gamma_{pe xrav}$	$1.13^{+0.11}_{-0.09}$
E_{fold}	100 keV
R_{refl}	80.3
$\cos i$	0.5 fixed
N_H^3	$5.0 \times 10^{26} \text{ cm}^{-2}$
Γ_3	$2.3^{+0.18}_{-0.89}$
χ^2	0.99
$E_{FeK\alpha}$	6.05 keV
E_{O8}	0.53 keV
E_{O8}	0.57 keV
E_{O8}	0.65 keV

NOTE. — The best fit model consists of the following: three power laws with tied photon indices absorbed by N_H^1 , N_H^2 , and N_H^3 ; cold reflection modeled by *pe xrav*; and four gaussian components whose emission line strengths are given. All components are absorbed by N_H^{Gal} .

gaussian components, all of which are obscured by galactic absorption. The FeK α emission line presence in the spectrum suggests the addition of a reflection continuum which we modeled with *pe xrav*. *pe xrav* is an exponentially cut off power law spectrum reflected from neutral material in which we fixed the abundances to solar values. The sum of the cut off power law and the reflection component represent the output spectrum. Table 1 presents the parameters for this fit.

In agreement with Sambruna et al., we have shown that the X-ray emission from the radio galaxy 3C 445 is very complex. The properties of this galaxy's emission

are quite similar to those of type 2 radio-quiet AGNs (Sambruna et al. 2007). This is interesting, because 3C 445 is a radio-loud AGN and this is the first time such features have been detected in a BLRG (Sambruna et al. 2007). Although not the main focus of our study, a quick look at the AGN of 3C 445 provides reasons for future research.

5. DISCUSSION

The results from the summer are mainly concerned with the southern hot spot of 3C 445. The fitted spectrum, the contour plot created in the X-ray and overlaid in the infrared, and the Compton Sphere models of the emission within the hot spot represent the bulk of our findings. In addition, there is a fitted spectrum of the AGN.

The differences in the structure of the hot spot in the X-ray and infrared (Figure 1) have interesting implications for its emission mechanisms. Up to this point, synchrotron emission has been assumed for the hot spot. However, given the differences in morphology between the X-ray and infrared emission, it is difficult to account for the X-ray emission as synchrotron emission from either the same population of electrons that produces the infrared emission, or a population of electrons that is strongly linked to the infrared emission. In either case we would expect to see an X-ray morphology very similar to that seen in the infrared. However, as shown in Figure 1, the morphology in these two bands differ strongly. X-ray synchrotron emission would therefore require a second electron population that would be spatially displaced from that seen in the infrared, and in particular located closer to the core (i.e., upstream from the shock at the hotspot) than the infrared emission. Such a model is difficult to reconcile with the image, since under the usual model of hotspots (Hardcastle et al. 2004) the most energetic emission should come from the immediate shock region. A second argument in favor of interpreting the X-ray emission as coming from lower-energy electrons is as follows: Not only is it difficult to join the X-ray emission with the IR and also reproduce the observed spectral index, but also the fact that the spectral power appears to increase with photon energy, combined with a smooth rather than knotty morphology, indicates that the emission appears to come from lower-energy electrons.

For these reasons, we believe that it is more consistent to propose that inverse-Compton (IC) scattering is occurring within the hotspot, as modeled in Figures 4 and 5. The models shown in those Figures assume that the origin of the IC component is from the synchrotron self-Compton process, in which the photon being scattered originates within the jet. Table 2 shows the parameters for the models shown in Figures 4 and 5. The two main differences are the different values of γ_{min} as well as differing magnetic fields; in Figure 4, equipartition (equal amounts of emission in the magnetic field as in particles in the hot spot) is assumed, and in Figure 5 this is no longer the case. In both models, the left curves represent the synchrotron emission while the right curves model the IC emission. On the left curve, the crosses represent points estimated from Brunetti et al. (2003), and the diamonds were calculated from Prieto et al. (2002). We found our X-ray data point from the best fit line $y=0.1784x+41.188$ obtained from four

TABLE 2
COMPTON SPHERE MODEL PARAMETERS

Figure	B (G)	L (erg/s)	γ_{max}	γ_{min}
4	3×10^{-5}	1.5×10^{43}	1×10^6	4.5×10^3
5	3×10^{-6}	2×10^{45}	4×10^6	1×10^3

NOTE. — Table 2 presents the model parameters used in the Compton Sphere Suite. Because we changed the magnetic field between the two models, several of the other parameters had to be tweaked as well. In changing the magnetic field in Figure 4 from that used by Prieto et al. (2002), equipartition is no longer assumed.

points giving the flux at different energies. This is represented by the solid line. The two dashed lines represent the errors in our spectral fit and are represented by the lines $y=0.5584x+41.188$ and $y=-.1616x+41.188$.

There are three curves that make up the IC portion of both models. The dotted curve represents Comptonization of cosmic microwave background photons in the jet. The solid curve represents the first collision from Comptonization of photons under the synchrotron self-Compton process emitted within the jet by particles within the jet. In more luminous sources, multiple collisions do occur. The red curve represents the sum of all Comptonization reactions. The IC portion of the model is dominated by the solid black curve. It should also be noted that the x-axis refers to the energy in terms of the rest mass of the electron, so that 0 corresponds to 511 keV.

As can be seen, the equipartition model (Figure 4) fails to reproduce all the data points, underpredicting the X-ray emission by many orders of magnitude. One can do a better job of reproducing the X-ray flux only if the magnetic field is decreased and the minimum energy of the particles is also decreased. However, even that model, in which the jet is out of equipartition by a factor 10, fails to reproduce the data, as it overpredicts the

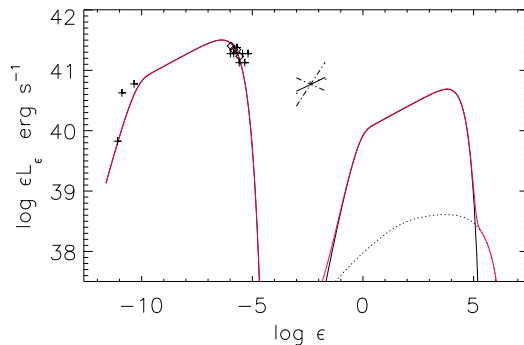


FIG. 4.— A model of the multiwaveband emission from the southern hotspot, obtained with the Compton Sphere suite. See §5 for details. This is a plot of luminosity versus photon energy, however the units of X-axis are in electron rest masses, so that 0 corresponds to 511 keV. Data points from the VLA, VLT and *Chandra* data are shown, along with errors on spectral index. The lower-frequency red curve refers to the modelled synchrotron emission, while the dotted curve represents Comptonization of cosmic microwave background photons in the jet. The solid curve represents the first collision from Comptonization of photons under the synchrotron self-Compton process emitted within the jet by particles within the jet. In this version of the Compton Sphere model, equipartition is assumed. The synchrotron emission is modeled fairly accurately, but because equipartition is assumed, our X-ray data point does not fit with the model.

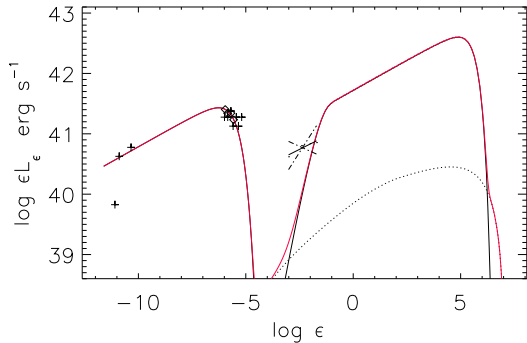


FIG. 5.— The x-axis refers to the energy in terms of the rest mass of the electron, so that 0 corresponds to 511 keV. In this version of the Compton Sphere model, equipartition is not assumed by the fact that the magnetic field has been decreased. The data points mostly fit the synchrotron portion of this model, with one outlier. This outlier is caused by the increased γ_{min} value from Figure 4. The X-ray data point is close to fitting the IC portion of the model.

lowest frequency radio point by an order of magnitude and is also not consistent with the X-ray spectral index. Because neither model fit quite right with all the data points, there is reason for future work on this project. The main goal will be to find a better way to model the data points, perhaps the upstream Comptonization model (Georganopoulos 2004). In this model, the gradual slowdown of these powerful extragalactic jets all the way out to the hot spot is taken into account. As a result of the jet deceleration, the CMB photon energy density in the flow decreases as well causing the X-ray brightness to decrease (Georganopoulos 2004). Perhaps a model of this form would better fit our data.

6. CONCLUSIONS

By extracting the spectrum and fitting it to a simple power law with galactic absorption, we have shown that synchrotron emission is present within the southern hot spot of radio galaxy 3C 445 (Hardcastle et al. 2004). By

overlaying the X-ray contours to the VLA image, it immediately became clear that the X-ray structure of the hot spot was different from that seen in the infrared. Where there appears to be only one region in the X-ray, there are three distinct regions in the infrared, and the maximum in the X-ray does not correspond to any of the bright regions in the infrared. This is impossible with just the simple synchrotron model we determined from the hot spot spectrum (Hardcastle et al. 2004). Therefore, we are proposing a model with both synchrotron and IC emission coming from this hot spot.

While we have determined that both synchrotron and IC emission are present, we are still working on accurately modeling this emission. If equipartition is assumed as in Figure 3, the X-ray data point does not fit the model. Even when the magnetic field is decreased and equipartition is no longer assumed, our model is still not entirely accurate. Perhaps another type of model is necessary.

As a side note, the fit to the AGN spectrum makes 3C 445 an even more interesting object to study. The scope of this project did not include such tasks as investigating the AGN's gas content or determining the density and mass of the warm medium within it (Sambruna et al. 2007). These provide possibilities for further research.

This project was funded by a partnership between the National Science Foundation (NSF AST-0552798), Research Experiences for Undergraduates (REU), and the Department of Defense (DoD) ASSURE (Awards to Stimulate and Support Undergraduate Research Experiences) programs. Support for this work was provided by the National Aeronautics and Space Administration through Chandra Award Number G07-8114A, issued by the Chandra X-ray Observatory Center, which is operated by the Smithsonian Astrophysical Observatory for and on behalf of the National Aeronautics and Space Administration under contract NAS8-03060.

REFERENCES

- Brunetti, G., Mack, K.-H., Preito, M., & Varano, S. 2003, MNRAS, 345, L40
 Georganopoulos, M., & Kazanas, D. 2003, ApJ, 589, L5
 Georganopoulos, M., & Kazanas, D. 2004 ApJ, 604, L81
 Georganopoulos, M., Kazanas, D., Perlman, E., Wingert, B., Graff, P. & Castro, R. *The Compton Sphere* The Compton Shoppe. 5 Apr. 2007. 23 July 2008. <http://jca.umbc.edu/markos/cs/index.html>
 Hardcastle, M. J., Harris, D. E., Worrall, D. M., & Birkinshaw, M. 2004, ApJ, 612, 729
 Harris, D. E., & Krawczynski, H. 2006, ARAA, 44, 463
 Longair, Malcolm. High Energy Astrophysics. 2nd ed. Vol. 1. New York: Cambridge UP, 1992. 100-105
 Longair, Malcolm. High Energy Astrophysics. 2nd ed. Vol. 2. New York: Cambridge UP, 1994. 229
 Prieto, A., Brunetti, G., & Mack, K. 2002, Science, 193.
 Sambruna, R. M., Reeves, J. N., & Braitto, V. 2007, ApJ, 665, 1030